Spin–orbit induced coupling of charge current and spin polarization



2004 J. Phys.: Condens. Matter 16 R179

(http://iopscience.iop.org/0953-8984/16/7/R02)

INSTITUTE OF PHYSICS PUBLISHING JOURNAL OF PHYSICS: CONDENSED MATTER

J. Phys.: Condens. Matter **16** (2004) R179–R207 PII: S0953-8984(04)57352-6

**TOPICAL REVIEW**

# Spin–orbit induced coupling of charge current and spin polarization

**Robert H Silsbee**

Department of Physics, Cornell University, Ithaca, NY 14853-2501, USA

E-mail: RHS1@cornell.edu

Received 13 October 2003
Published 6 February 2004
Online at stacks.iop.org/JPhysCM/16/R179 (DOI: 10.1088/0953-8984/16/7/R02)

**Abstract**

In systems without inversion, symmetry spin–orbit interactions couple the charge–current and spin-polarization degrees of freedom. This review gives a brief summary of the origins of this coupling and reviews a variety of ways in which the coupling may be made evident experimentally, with emphasis on the detection of electric-field driven spin polarization.

## Contents



  

## 1. Introduction

In systems lacking inversion symmetry, associated with either the crystalline structure or the physical configuration, the spin degeneracy of Bloch states may be removed by the spin–orbit interaction. The remaining degeneracy of the two states $|\boldsymbol{k}\uparrow\rangle$ and $|-\boldsymbol{k}\downarrow\rangle$, required by time-reversal symmetry in the absence of magnetic fields, implies a connection between wavevector and spin which leads to surprising correlations of spin polarization and charge current. An applied electric field induces not only a charge current but also a spin polarization. Conversely the generation of a non-equilibrium spin polarization typically results simultaneously in a charge current. The effects discussed in this review are, of course, in addition to the many important consequences of the spin–orbit splitting of the valence band states of typical semiconductors at $k = 0$.

The emerging field of spintronics has focused primarily on issues of spin injection and detection in semiconductor systems and magnetoresistance and related phenomena in inhomogeneous metallic systems. In semiconductors with large spin–orbit splittings the coupling of spin polarization with electric fields or currents offers new opportunities for spin manipulation in both electronic and optoelectronic devices. With these possibilities in mind, this review will focus primarily on systems confined to two-dimensions, where the relevant splittings are much larger than in three-dimensional systems, and to degenerate gases (Fermi systems) of electrons or holes. Much of the early theoretical work focused more on three dimensions and classical gases (Boltzmann systems) but most of the basic physics is very much the same and often simpler for the degenerate two-dimensional electron gas (2DEG). Our discussion also focuses on behaviour in the absence of applied magnetic fields. With the application of a magnetic field, there arises a rich spectroscopy of 'combined resonance' experiments, reviewed by Rashba [1], in which the spin splittings play a critical role, and there are many experiments, referenced in table 1, which are influenced by the splitting and can yield values of the splitting parameter.

We start with a review of the spin–orbit splitting and its implications for the electron dispersion relations and one-electron eigenstates, first in three dimensions and then, in more detail, in two-dimensional systems. Critical is the coupling between wavevector and spin orientation of the eigenstates. In exploring the experimental ramifications of this coupling, we first look at the spin polarization produced in association with a charge current by application of an electric field and how that polarization might be detected. It is natural then to consider the converse problem, the excitation of spin polarization and the detection of the associated charge currents. Since this second topic was recently reviewed by Ganichev and Prettl [2], we restrict the discussion here to a brief summary of the essential ideas, a few very recent results, and mere mention of the number of relevant issues.

## 2. Band structure with spin–orbit splitting

### *2.1. Spin–orbit splittings in three dimensions*

As suggested already the key to connecting spin accumulation with charge currents is the correlation, in the electronic eigenstates, of wavevector with spin orientation. Time reversal symmetry leads to the Kramers theorem requiring that a state of spin-up and wavevector $\boldsymbol{k}$ must be degenerate with the spin-down state of wavevector $-\boldsymbol{k}$, $E(\boldsymbol{k}\uparrow) = E(-\boldsymbol{k}\downarrow)$, but in the absence of inversion symmetry we may expect $E(\boldsymbol{k}\uparrow) \neq E(-\boldsymbol{k}\uparrow)$ and $E(\boldsymbol{k}\uparrow) \neq E(\boldsymbol{k}\downarrow)$. As a consequence, non-equilibrium occupation of states of particular spin will be associated with non-equilibrium occupation of states of related wavevector: there may be an association

of charge current and spin polarization. We must first explore the energy dispersion relations for systems exhibiting this lifting of the spin degeneracy. In particular, our interest is in spin-dependent terms in the energy which are linear or cubic in the wavevector.

Dresselhaus [3] has shown, for the electronic states in the zinc blende structure, the existence of splittings linear in $k$ for the heavy/light hole band and cubic in $k$ for the conduction and split-off hole bands. The spin–orbit energies for the conduction band states, for example, are given by

$$E_{\mathrm{SO}} = \pm\gamma[k_x^2(k_y^2 - k_z^2)^2 + k_y^2(k_z^2 - k_x^2)^2 + k_z^2(k_x^2 - k_y^2)^2]^{1/2}, \tag{1}$$

corresponding to interaction of the spin with an effective magnetic field

$$\boldsymbol{H}_{\mathrm{SO}} = (2\gamma/g\beta)[\hat{\boldsymbol{x}}k_x(k_y^2 - k_z^2) + \hat{\boldsymbol{y}}k_y(k_z^2 - k_x^2) + \hat{\boldsymbol{z}}k_z(k_x^2 - k_y^2)], \tag{2}$$

with $\beta$ the Bohr magneton, $g$ the $g$-factor for the Zeeman splitting and $\gamma$ a measure of the strength of the spin–orbit splitting. The coordinate axes are the cubic axes of the crystal. The effective field is perpendicular to the wavevector $\boldsymbol{k}$ and of a magnitude which depends upon the direction of $\boldsymbol{k}$. In particular it is zero for $\boldsymbol{k}$ along the (111) and (100) symmetry directions. This contribution to the spin splitting, either in three dimensions or the contribution derived from it in two dimensions, is often referred to as the Dresselhaus term. The prediction of this term was confirmed in bulk GaSb by Seiler *et al* [4] based on the beating pattern in Shubnikov–de Haas oscillations, the technique which has become the most common in characterizing the spin splittings in both three- and two-dimensional systems.

A useful review of bulk spin splittings in cubic III–V compounds is given by Pikus *et al* [5], including both theoretical expressions for the splitting constants in terms of material parameters and experimental values determined from spin relaxation measurements. The discussion includes the implications of the reduction of the tetrahedral symmetry of the zinc blende structure by application of a uniaxial stress: in this case spin–orbit terms linear in $k$ become symmetry allowed for the conduction and split-off valence bands as well as for the heavy/light hole band [6].

The lower symmetry of the wurzite structure allows spin–orbit splittings of the conduction band states linear in $k$ as noted by Rashba [7–10] and independently by Casella [11]. These are in addition to cubic terms similar to those of the zinc blende case, though with appropriately lowered symmetry. The symmetry-allowed linear splitting is represented as an added term, a 'Rashba term', in the Hamiltonian,

$$\mathcal{H}_{\mathrm{SO}} = \alpha\boldsymbol{\sigma} \cdot (\boldsymbol{k} \times \hat{\boldsymbol{z}}), \tag{3}$$

where $\boldsymbol{\sigma}$ is the vector of the Pauli spin matrices, $\hat{\boldsymbol{z}}$ a unit vector in the direction of the threefold symmetry axis of the crystal and $\alpha$ a parameter describing the strength of the spin–orbit splitting. Again this term may be interpreted as the interaction of the electron spin with an effective magnetic field,

$$\boldsymbol{H}_{\mathrm{SO}} = (2\alpha/g\beta)(\boldsymbol{k} \times \hat{\boldsymbol{z}}), \tag{4}$$

which is often referred to as the Rashba field. We will frequently speak of the splitting in terms of the corresponding frequency $\omega_{\mathrm{SO}} \equiv g\beta|\boldsymbol{H}_{\mathrm{SO}}|/\hbar = 2\alpha|\boldsymbol{k}|/\hbar$, the precession rate of the spin in the spin–orbit field.

### *2.2. Spin–orbit splittings in two dimensions*

Of particular interest in this review are experiments on samples with electrons or holes confined to two dimensions, the two-dimensional electron gas or 2DEG. We give only a brief introduction here: a comprehensive review is given by Zawadzki and Pfeffer [12]. Restricting the discussion

to spin splittings which are linear in $k$ we find two possible symmetries for the spin–orbit term of the effective Hamiltonian:

$$\mathcal{H}_{\mathrm{D}} = \alpha(k_x\sigma_x - k_y\sigma_y) \tag{5}$$

$$\mathcal{H}_{\mathrm{R}} = \alpha(k_x\sigma_y - k_y\sigma_x), \tag{6}$$

where we have assumed a (100) or (111) direction of growth for equation (5). Terms of the form of equation (5) are conventionally referred to as Dresselhaus or bulk-inversion-asymmetry (BIA) terms, and of the form equation (6) as Rashba or structure-inversion-asymmetry (SIA) terms. Both the Dresselhaus term, for (001) or (111) growth directions, and the Rashba term give energy splittings isotropic in the confining plane.

Terms of the Dresselhaus form typically derive from the $k^3$ spin–orbit term, equation (1), of the bulk band structure [13–15]. In a quantum well with infinite barrier height the confinement of the electron wavefunction in the growth direction forces quantization of the corresponding component of the wavevector. For the case of the lowest subband, normally the only case of interest, this implies $|k_{\mathrm{growth}}| = \pi/b$ where $b$ is the thickness of the well. If this value is used in the expression equation (1) we obtain an expression for the spin splitting of the 2DEG as a function of wavevector in the plane of the well. If the growth direction is along the cubic axis $\hat{z}$ this gives

$$E(k_x, k_y) = \pm\gamma\left[\left(\frac{\pi}{b}\right)^4 (k_x^2 + k_y^2) - 4\left(\frac{\pi}{b}\right)^2 k_x^2 k_y^2 + k_x^2 k_y^2 (k_x^2 + k_y^2)\right]^{1/2} \tag{7}$$

$$\stackrel{b\to 0}{\longrightarrow} \pm\gamma\left(\frac{\pi}{b}\right)^2 (k_x^2 + k_y^2)^{1/2}. \tag{8}$$

In the limit $(\pi/b)^2 \gg (k_x^2 + k_y^2)$ the corresponding effective field is

$$\boldsymbol{H}_{\mathrm{SO}} = \frac{2\gamma}{g\beta}\left(\frac{\pi}{b}\right)^2 (-\hat{\boldsymbol{x}}k_x + \hat{\boldsymbol{y}}k_y). \tag{9}$$

The parameter $\alpha$ of equation (5) for the 2DEG is related to the parameter $\gamma$ for the three-dimensional systems by $\alpha = (2\gamma/g\beta)(\pi/b)^2$. In the limit of narrow wells the splitting is isotropic in the plane of the well, but inclusion of the terms cubic in the in-plane wavevector gives a more complicated effective field and the splittings become anisotropic [14, 16, 17]. The anisotropy terms will be important for Fermi wavevectors comparable with the confinement parameter $\pi/b$ or, equivalently, for Fermi energies of the order of the splittings of the subbands produced by the confining potential.

For other growth directions equation (1) must be transformed to a coordinate frame with one basis vector parallel to the growth direction [14]. For most growth directions this gives anisotropy in the plane of the well even for the *linear* Dresselhaus term. For quantum wells with finite barrier heights, as well as for heterojunction wells, the wavefunction spills from the well into the bulk and the constant $\gamma$ is replaced by a suitable average of the bulk splitting parameter in the well and the bulk [14]. This can provide a means of modulating the spin splitting since gating the sample will change the relative weights of the well and barrier region in calculating the average $\gamma$ [14].

A different mechanism contributing to the spin splittings has recently been recognized. Consider two semiconductors 1 and 2 and denote successive layers in the growth direction as C1 or C2 for the cation layers and A1 or A2 for the anion layers. Consider the two quantum wells denoted by the structures

$$\cdots \mathrm{A1–C1–A1–C1–A1–C1–A1{=}C2–A2–C2–A2–C2–A2–C2–A2{=}C1–A1–C1–A1–C1}\cdots \tag{10}$$

and

$$\cdots \text{A1–C1–A1–C1–A1–C1–A1=C2–A2–C2–A2–C2–A2–C2=A1–C1–A1–C1–A1–C1}\cdots, \tag{11}$$

with the double bar indicating the position of the interface. In conventional quantum well growth, the growth occurs on saturated anion surfaces. Thinking in terms of growth from left to right, the first structure above will be the expected structure with an A1–C2 interface on the left side of the well and an A2–C1 interface on the right. Thus the full quantum well structure is not symmetric under inversion in the plane in the centre of the well. The second structure, with interfaces A1–C2 and C2–A1, *is* symmetric but is *not* the structure to be expected in MBE growth. In [19] it is shown experimentally that the barrier heights for the two interfaces A1–C2 and A2–C1 are different for many semiconductor pairs. This intrinsic structural asymmetry of the well leads to terms of both Dresselhaus and Rashba symmetry [20–22]. There will be a contribution to the Rashba term, discussed below, from the asymmetry associated with a difference in height of the two barriers, and a Dresselhaus term arises from the detailed microscopic structure of the interfaces as discussed in [20, 21].

Although spin splitting of the Rashba symmetry is forbidden for the bulk tetrahedral zinc blende structure, Bychkov and Rashba [8, 23] noted that such a term is allowed for a 2DEG confined in a well lacking inversion symmetry in the growth direction. Such asymmetry arises naturally in inversion layers, heterojunctions and asymmetric quantum wells. Sources of asymmetry of quantum wells include asymmetric doping profiles, differing chemical or alloy compositions of the confining materials on either side of the well, electric fields applied via front or back gates, and the barrier height difference associated with the inequivalence of the A1–C2 and A2–C1 interfaces noted already. A selection of references [16, 107, 25–28] indicate the variety of issues involved in the calculation of the Rashba parameter, and Pfeffer and Zawadzki [12, 29] in particular note serious problems with the common assertion that the splitting is simply proportional to the average electric field.

The Rashba term gives an isotropic splitting, independent of the direction of $\boldsymbol{k}$ in the plane of the 2DEG, as does the linear Dresselhaus term for (001) and (111) growth directions. However, as we shall note in section 2.3, if the terms of both symmetries are of comparable importance the interference between the two can give rise to anisotropic splitting even though the individual terms are isotropic [14, 30]. Several factors influence the relative importance of the two, with strong confinement, large band gap, and symmetric confinement favouring Dresselhaus over Rashba. Recent experimental results [17, 18, 31, 32] displaying the effects of interference between the two terms, in both GaAs and InAs wells, indicate that the two terms can easily be of comparable magnitude.

Although the spin splitting is revealed in a number of contexts it is most often determined experimentally by analysis of Shubnikov–de Haas oscillations of resistivity with magnetic field [33, 34]. The two spin subbands, see section 2.3, each give their own set of oscillations and the beat pattern from their interference, along with the mean period, allows determination of the carrier density and the spin splitting at the Fermi energy [35–37]. The following list illustrates the variety of additional experiments which evidence the spin splitting. Table 1 gives a sampling of the experimentally determined spin splitting parameter for a number of systems. The codes in the 'Expt' are keyed to the folliwng list of techniques, which also gives references to a few selected papers illustrating each.

- SdH—Shubnikov–de Haas oscillations [34, 35, 37]
- CO—commensurability oscillations [38]
- WL/AL—weak-localization/anti-localization [18, 32, 39, 40]

**Table 1.** Spin splittings for a number of quantum well systems. The 2DEG is primarily in the centre material if three are listed, in the second if only two. The experimental method is coded according to the symbols in the list of techniques in the text. Values in parenthesis are estimated from parameters quoted in the references.

| System | $n/p$ ($10^{12}$ cm$^{-2}$) | $b$ (Å) | Expt | $\alpha$ ($10^{-9}$ eV cm) | $2\alpha k_F$ (meV) | References |
|---|---|---|---|---|---|---|
| CdTe/HgTe/CdTe | $n = 0.5$–$1.3$ | 115 | SdH, CR | 2.7–4.3 | (10–25) | [44] |
| Insulator/Si | $p = 0.8$–$2.8$ | ? | SdH | 1 | (4.5–8) | [36] |
| AlGaAs/GaAs | $n = 0.2$–$0.7$ | ? | WL/AL | (0.03–0.04) | 0.07–0.16 | [32] |
| $Al_{0.33}Ga_{0.67}As/GaAs$ | $n = 1.3$ | 170 | RS | (0.4) | 0.22 | [17] |
| $Al_{0.3}Ga_{0.7}As/GaAs$ | $n = \sim 0.3$ | ? | ESR | 0.25 | (0.7) | [43][a] |
| $Al_{0.5}Ga_{0.5}As/GaAs$ | $p = 0.5$ | ? | CR | 0.6 | (2) | [42][a] |
| $In_{0.52}Al_{0.48}As/In_{0.53}Ga_{0.47}As$ | $n = 1.6$–$2.4$ | ∼100 | SdH | 0.8–0.6 | 5.8–4.9 | [45] |
| $InAlAs/In_{0.53}Ga_{0.65}As/InGaAs$ | $n = 1.7$ | 150 | SdH | (0.36) | 2.37 | [34] |
| $In_{0.5}Ga_{0.5}/In_{0.77}Ga_{0.23}As/InP$ | $n = 0.6$ | 100 | SdH | 0.5 | (1.9) | [26] |
| $InP/In_{0.77}Ga_{0.23}As/InP$ | $n = 0.5$–$0.8$ | 140 | SdH | 1.1–0.7 | (3.9–3.1) | [26] |
| $InP/In_{0.77}Ga_{0.23}As/InP$ | $n = 0.7$–$1.6$ | 100 | SdH | 1.5–0.6 | (6.3–3.8) | [25] |
| InAs (complex well) | $n = 0.75$–$1.15$ | ∼100 | SdH | 2.1–4.5 | (9–24) | [46] |
| AlSb/InAs/AlSb | $n = 1.1$–$2.0$ | 150 | SdH | 0.6 | 3.2–4.5 | [47] |
| AlSb/InAs/AlSb | $n = ?$ | 150 | WL/AL | — | 0.4 | [48] |
| AlSb/InAs/AlSb | $n = 1.0$ | 75 | SdH | 0.9 | 4 | [35] |
| AlSb/InAs/AlSb | $n = 1.1$ | 100 | SdH | 3.3 | 15 | [35] |
| Insulator/InAs | $n = 1.2$–$2.4$ | ? | SdH | 1–4 | (5–24) | [49] |

[a] As interpreted in [23].

- IR—infra-red absorption [41]
- RS—Raman scattering [17]
- ESR—electron spin resonance [42]
- CR—combined resonance [1, 43].

The ability to modulate the magnitude of the Rashba splitting by using a gated structure is necessary to realize the spin transistor proposed by Datta and Das [50]. The gating influences the observed spin splitting through changes in both the Rashba parameter and the Fermi wavevector as the carrier concentration is changed. The effect of the gating on the Rashba constant is complex, involving both changes in the potential distribution and the distribution of the electron density within the well and the spillover into the barrier regions. A number of authors [25, 26, 45, 46, 51] have reported successful gate-modulation of the Rashba spin splitting with a tunable range of up to a factor of five. Lu *et al* [52] probed the spin splitting of a p-type symmetrically doped GaAs quantum well as a function of gate voltage. The symmetry of the structure allowed access to both negative and positive values of the Rashba parameter. They achieved a population difference of the two subbands of roughly 20% of the electron density, corresponding to a spin splitting of about 20% of the Fermi energy at a hole concentration of $5 \times 10^{11}$cm$^{-2}$.

### *2.3. Fermi lines and quantization axes*

Understanding the correlation of spin quantization axes with the electron wavevector provides the key to the connection between electric current and spin polarization. Let us examine the band structure for the 2DEG for the two simple examples of spin splittings described in section 2.2.

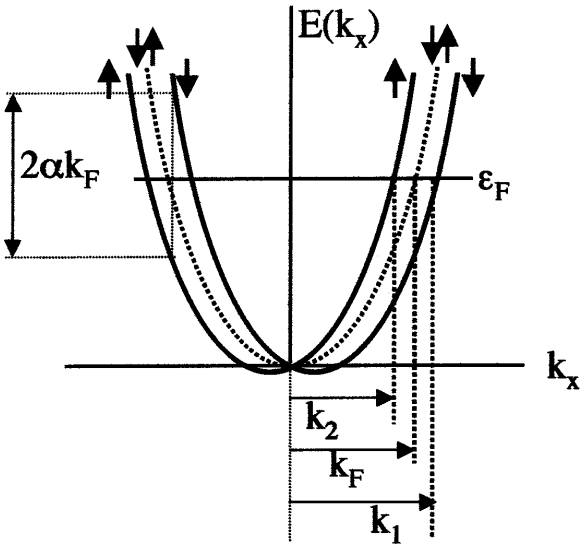


**Figure 1.** Energy dispersion relation for: unsplit bands—dotted line; spin–orbit split bands—solid lines.

Figure 1 illustrates the dispersion relation for the 2DEG,

$$E(k) = \frac{\hbar^2}{2m^*}k^2 \pm \alpha k, \tag{12}$$

appropriate to an isotropic splitting linear in $k$, such as implied either by the small $k$ limit of the Dresselhaus term for (001) or (111) growth direction, equation (8), or by the Rashba term equation (3), with $k$ the magnitude $(k_x^2 + k_y^2)^{1/2}$ of the two-dimensional wavevector $\boldsymbol{k} = \hat{\boldsymbol{x}}k_x + \hat{\boldsymbol{y}}k_y$. Rotation of the curves of figure 1 about the energy axis generates the energy surface $E(\boldsymbol{k})$. The two states for a given $\boldsymbol{k}$ correspond to quantization of the electron spin antiparallel or parallel to the spin–orbit effective field.

For a Fermi degenerate gas of carriers, at zero temperature these states are filled to the Fermi energy $\epsilon_F$, corresponding to Fermi wavevectors

$$k_1 = (1 + \eta)k_F \qquad k_2 = (1 - \eta)k_F, \tag{13}$$

with $k_F = \sqrt{2\pi n}$ the Fermi wavevector appropriate in the absence of the spin–orbit term for the 2DEG with carrier concentration $n$. The dimensionless parameter $\eta$ characterizing the difference in radii of the two Fermi discs is related to the spin–orbit splitting parameter $\alpha$ by the relation

$$\eta = \frac{\alpha k_F}{2\epsilon_F}. \tag{14}$$

Working only to first order in $\eta$, as we shall throughout this review, the full spin splitting of the states at the Fermi wavevector is

$$\epsilon_S = 2\alpha k_F = 4\eta\epsilon_F. \tag{15}$$

The Fermi velocities for the two subbands $v_{Fi} = \hbar k_F/m^* \equiv v_F$ are the same and are *not* given by $\hbar k_i/m^*$!

We may represent the filling of the $\boldsymbol{k}$ states, for Rashba symmetry, by the plot of figure 2(a) in which the two shaded discs represent the Fermi seas associated with the two branches

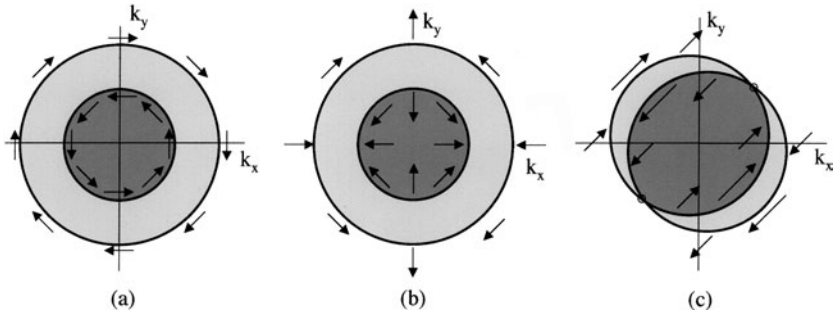


**Figure 2.** Fermi discs and spin quantization directions for spin–orbit split bands. Light shading if only states in band 1 are occupied; heavy shading if states in both bands are occupied. (a) Rashba symmetry; (b) Dresselhaus symmetry; (c) equal amplitudes of Rashba and Dresselhaus terms: splitting is zero in the (11) direction and maximum in the $(1\bar{1})$ direction.

of the dispersion relation and the two circles, the corresponding Fermi lines. The arrows denote the orientation of the spin eigenstates, either parallel or antiparallel to the Rashba field, $\boldsymbol{H}_{\mathrm{SO}} = (2\alpha/g\beta)(\boldsymbol{k}\times\hat{z})$, associated with the wavevector $\boldsymbol{k}$. Essential to note is the correlation of spin orientation with wavevector direction. In disc 1, for example, electrons at the Fermi energy moving to the right are dominantly polarized in the negative $y$-direction while those moving to the left are polarized in the positive $y$-direction, etc. As a result, any displacement of the disc in $k$-space results in a correlated change in both charge current and spin polarization. The interesting phenomena are typically the result of incomplete cancellation of contributions from the two discs because of their different size, characterized by the parameter $\eta$. In equilibrium there is of course neither net polarization of the spins nor a charge current. We will address the question of the existence of an equilibrium spin-polarized current in section 3.4.

Figure 2(b) shows the two Fermi discs and the associated spin orientations for the case of dominance by the linear Dresselhaus term, for a (001) or (111) grown well. Again the splitting is isotropic but here we have $x$-polarization of spins moving in the $x$-direction rather than $y$-polarization, and no longer the simple rule that the quantization axis for the spins is perpendicular to the wavevector.

The situation becomes more complex if the Rashba and Dresselhaus terms are comparable in strength [16, 17, 30]. Figure 2(c) illustrates the case for equal strengths of the two terms. Although for either the splitting is isotropic, the interference between the two results in anisotropy of the spin splitting. Comparison of the spin orientations in figures 2(a) and (b) shows the source of the interference: in the (10) and (01) directions the spin–orbit fields add in quadrature, while in the $(1\bar{1})$ and (11) directions they interfere constructively and destructively, respectively. For other growth orientations these anisotropies can become even more dramatic [14]. As already noted, the interference of the two terms has been demonstrated in a number of experiments [17, 31, 32].

## 3. From charge current to spin polarization

Perhaps the most striking consequence of the $\boldsymbol{k}$-dependent spin splittings is the implication that an applied electric field should induce not only a charge current but also a spin polarization, an effect suggested in passing by Ivchenko and Pikus [53] in 1978. The suggestion has been considered theoretically in more detail by Aronov *et al* [54, 55], Edelstein [56], Chaplik *et al* [57] and Inoue *et al* [58]. Johnson [59], in 1998, proposed an experiment to demonstrate the presence of the electric-field induced spin polarization.

### *3.1. Relaxation times*

The relative magnitude of various relaxation times are critical in defining appropriate models for our discussion: in particular the spin $\tau_S$ and momentum or resistivity $\tau_\rho$ times. Unless explicitly stated we assume the spin relaxation to be via the D'yakonov–Perel (DP) mechanism [60–62] in which the spin relaxation is the result of the interplay of the resistivity scattering and the spin precession in the spin–orbit field. We think of a series of resistivity collisions interspersed with periods of free precession about the spin–orbit field whose orientation is determined by the current wavevector. Note that the collisions themselves in the DP mechanism do *not* involve a spin flip.

In the case of strong collisions, which we shall denote as the 'dirty limit', we have $\omega_{SO}\tau_\rho \ll 1$: the accumulated precession angle between successive collisions is small and there is little loss of spin memory per collision. In these successive inter-collision periods the spin–orbit field is randomly related to that of the previous period so that the spin executes a random walk with a 'step length' $\sim\omega_{SO}\tau_\rho$. The mean square accumulated phase after a random walk for time $t$ is $\langle\delta\phi^2\rangle = (\omega_{SO}\tau_\rho)^2\, t/\tau_\rho$. Taking the spin relaxation time $\tau_S$ to be that value of $t$ for which the accumulated random phase is equal to unity we have the familiar motional narrowing result for the spin relaxation rate,

$$\tau_S^{-1} = \omega_{SO}^2\tau_\rho. \tag{16}$$

D'yakonov and Kachorovskii [13] extended the DP theory to the case of the two-dimensional confined system. Comparing equations (1) and (8) shows the ratio of the Dresselhaus spin–orbit energies $\hbar\omega_{SO}$ for the two- and three-dimensional cases to be $(\pi/bk_F)^2$. This implies, for the dirty limit, a substantial enhancement of the strength of the contributions from the Dresselhaus terms, by the order of $(\pi/bk_F)^4$. Note that in the two-dimensional system the fluctuating spin–orbit fields giving rise to the DP relaxation are in the plane of the 2DEG. Only the $x$-component of these fields contributes to the relaxation of the $y$-component of the spin and only the $y$-component contributes to the relaxation of the $x$-component of the spin. Both, however, contribute to relaxation of the $z$-component of spin and there arises a factor of two anisotropy of the spin relaxation. If the Rashba and Dresselhaus terms are equal in magnitude, the interference between the two can lead to very dramatic in-plane anisotropy of the spin relaxation. As can be seen from figure 2(c), with equal strengths of the two terms the spin–orbit field is *always* in the $\pm(11)$ direction and hence cannot contribute to relaxation of the spin-oriented parallel of (11). For a more detailed discussion, see the review by Averkiev *et al* [63] of spin relaxation in 2DEGs. There are, of course, other contributions to the spin relaxation involving a spin flip in the scattering. Unless explicitly included, these other processes will be assumed unimportant in the discussions below.

The 'clean limit', or the case of weak collisions, is characterized by $\omega_{SO}\tau_\rho \gg 1$: the precession in the spin–orbit field at a rate $\omega_{SO}$ gives a large precession angle during one resistivity scattering time. Every momentum scattering event results in substantial loss of spin memory: the spin and resistivity scattering times are effectively the same. In this regime we will make no distinction between the two times and refer simply to the scattering time $\tau$.

Table 2 will help determine whether to expect a sample to be in the clean or dirty limit. Expressions are given for the critical parameter $\omega_{SO}\tau_\rho$ for a reference sample defined by the parameter values in the first four rows. A number of other parameter values are listed as well. The formulae allow easy scaling to determine any of the parameters in terms of known mobility, spin–orbit coupling constant, concentration and carrier effective mass. Depending upon temperature, purity and spin–orbit strength, we may expect to find samples in either of the two regimes.

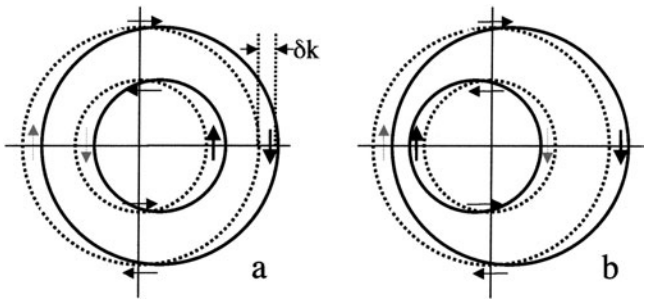


**Figure 3.** The Fermi discs for two non-equilibrium distributions. Dotted lines—equilibrium; solid lines—non-equilibrium. (a) Response to an applied electric field with $\delta k = q\mathcal{E}\tau/\hbar$; (b) response to spin injection. Heavier arrows denote added spins, lighter arrows depleted spins.

**Table 2.** System parameters for a 2DEG: the various parameters are expressed in terms of the mobility, Rashba constant, concentration and effective mass of the carriers. The last column gives the parameter values for a reference sample defined by the values in the first four rows.

| Parameter | Symbol | Formula | Units | Reference |
|---|---|---|---|---|
| Mobility | $\mu$ | $\mu$ | $\mathrm{cm}^2\ \mathrm{V}^{-1}\ \mathrm{s}^{-1}$ | $10^5$ |
| Spin–orbit constant | $\alpha$ | $\alpha$ | eV cm | $10^{-9}$ |
| Carrier concentration | $n$ | $n$ | $\mathrm{cm}^{-2}$ | $10^{12}$ |
| Effective mass ratio | $m^*$ | $m^*$ | — | $10^{-2}$ |
| Clean/dirty limit | $\omega_{\mathrm{SO}}\tau_\rho$ | $4.3\mu m^*\alpha\sqrt{n}$ | — | 4.3 |
| Fermi wavevector | $k_{\mathrm{F}}$ | $2.5\sqrt{n}$ | $\mathrm{cm}^{-1}$ | $2.5 \times 10^6$ |
| Fermi energy | $\epsilon_{\mathrm{F}}$ | $2.4 \times 10^{-12} n/m^*$ | meV | 240 |
| Fermi velocity | $v_{\mathrm{F}}$ | $2.9\sqrt{n}/m^*$ | $\mathrm{cm\ s}^{-1}$ | $2.9 \times 10^8$ |
| Spin splitting | $\epsilon_{\mathrm{S}} \equiv 2\alpha k_{\mathrm{F}}$ | $5\alpha\sqrt{n}$ | meV | 5 |
| Dimensionless coupling | $\eta$ | $5.3 \times 10^{14}\alpha m^*/\sqrt{n}$ | — | $5.3 \times 10^{-3}$ |
| Spin–orbit velocity | $v_\alpha \equiv \alpha/\hbar$ | $1.5 \times 10^{15}\alpha$ | $\mathrm{cm\ s}^{-1}$ | $1.5 \times 10^6$ |
| Scattering time | $\tau_\rho$ | $5.7 \times 10^{-16} m^*\mu$ | s | $5.7 \times 10^{-13}$ |

### *3.2. Clean limit*

To see how the application of an electric field can induce a spin polarization, consider first the clean limit. As suggested by figure 3(a), where we have taken the spin–orbit splitting to be of the Rashba symmetry, application of an in-plane electric field $\mathcal{E}$ gives, in steady state, a displacement of the two Fermi discs by an amount

$$\delta k_i = q\mathcal{E}\tau_i/\hbar, \tag{17}$$

where $\tau_i$ is the resistivity relaxation time, possibly different for the two Fermi discs. To avoid confusion of sign, the carriers are assigned a charge $q$ and qualitative arguments will be given in terms of a positive $q$. In subband 1 the electric field has, in net, transferred carriers from negative $k_x$ to positive and from spin-up to spin-down, giving a charge current and spin polarization. Subband 2 adds to the charge current but partially cancels the spin polarization. The subband contributions to the charge–current density and total spin density are

$$j_i = \frac{q^2\mathcal{E}\tau_i v_{\mathrm{F}} k_i}{4\pi\hbar} \tag{18}$$

$$S_i = \pm\frac{1}{2}\frac{q\mathcal{E}\tau_i k_i}{4\pi\hbar}, \tag{19}$$

with $i = 1, 2$ for the two subbands. In the scattering model of [64] the scattering times $\tau_i$ are related to the resistivity time $\tau$ by $\tau_i = \tau(1 \pm \eta)$. Using equations (13) and (14), the total charge current density in the $x$-direction becomes,

$$j = \frac{q^2 \lambda k_F}{2\pi\hbar}\mathcal{E}. \tag{20}$$

Adding the partially cancelling contributions of the two discs to the spin density gives for the spin polarization, $P \equiv 2(S_1 + S_2)/n$,

$$P = \frac{2q\tau\eta}{\hbar k_F}\mathcal{E} = \frac{q\tau\alpha}{\hbar\epsilon_F}\mathcal{E} \tag{21a}$$

$$= \frac{2\eta}{v_F}\frac{j}{nq} = \frac{\alpha k_F}{v_F\epsilon_F}\frac{j}{nq}. \tag{21b}$$

Equation (21$b$) relates the fractional spin polarization $P$ to the charge current density $j$ and we have expressed the results in terms of each of the parameters $\eta$ and $\alpha$. The density of states, at the Fermi level, for each disc is given to first order in $\eta$ by

$$D_i(E) = \frac{k_i}{2\pi\hbar v_F} = \frac{k_i}{k_F}\frac{n}{2\epsilon_F}, \tag{22}$$

proportional to its own Fermi wavevector $k_i$, and the velocity $v_F$ on the Fermi line is the same for both discs. Note that the contributions of the two discs add for the charge current but partially cancel for the spin polarization, the degree of cancellation determined by the dimensionless parameter $\eta = \alpha k_F/2\epsilon_F$. A large spin polarization to charge current ratio requires a large value of $\eta$: hence both a large Rashba splitting $\alpha$ and a small Fermi energy $\epsilon_F$. It is interesting to speculate on the possibility of achieving a value of $\eta$ equal to unity by going to a low enough, probably unrealistic, concentration that the radius of the smaller Fermi circle $k_2$ goes to zero. Though the quantitative arguments above rely on the assumption $\eta \ll 1$, it is still true that for values $\epsilon_F \leqslant \alpha k_F^2 m^*/2\hbar^2$ there is no longer the cancellation of spin polarization between the two subbands and the spin polarization is that given by equation (21$b$) with $\eta = 1$.

The results of equations (21$a$), (21$b$) depend on the assumption of elastic scattering rates from point-like impurities. An alternative assumption of equal scattering times for the two discs gives a spin polarization of a factor of two smaller [64, 65]. Similar expressions are quoted in [107, 55–58, 64] but with numerical factors varying over a range of a factor of $4\pi$.

### *3.3. Dirty limit*

With the scattering rate fast compared with the spin–orbit precession rate, a different plausibility argument [56] may be helpful. Again, for specificity, we take the Rashba form of the spin splitting.

As the carrier scatters rapidly from one $k$-state to another, in addition to the fluctuating Rashba field that gives rise to the DP spin relaxation, it feels a time averaged Rashba field proportional to its time average wavevector: $H_{\text{drift}} = 2\alpha\delta k/g\beta$ with $\delta k = q\mathcal{E}\tau/\hbar$. We will refer to this field as a 'drift spin–orbit field', a field proportional to the drift velocity of the carrier gas rather than to the individual carrier velocities. *Assuming* thermal equilibration in this effective field and using a Pauli susceptibility gives the same result, probably fortuitously, for the spin polarization as equation (21$a$). A lack of dependence of polarization on the resistivity time $\tau_\rho$ has been noted in several more formal calculations [56, 58] of equation (21$a$), again with simple point impurity scattering. Aronov *et al* [55] are critical of this plausibility argument and have properly calculated the electric field induced spin polarization, including a detailed treatment of the scattering. The results are similar in magnitude to equation (21$a$) but with

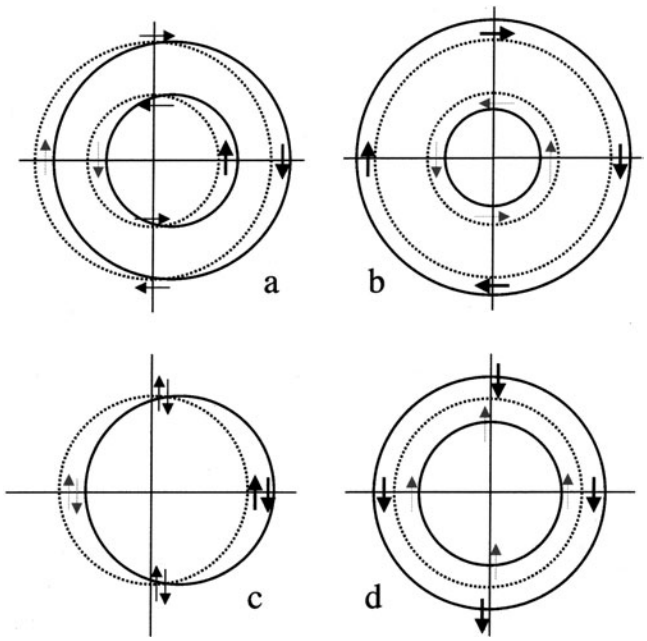


**Figure 4.** Four non-equilibrium situations, solid lines, compared with equilibrium, dotted lines. Heavier arrows denote added spins, lighter arrows depleted spins. (a) and (b) are for spin-split 2DEGs; (c) and (d) are for 2DEGs without spin splitting. (a) and (c) are the response to an applied electric field; (b) and (d) the effect of carrier transfer from one to the other spin subband.

numerical correction factors of order unity which depend upon the dominant spin relaxation mechanism.

An experiment of Kalevich and Korenov [66] attests to the utility of the concept of the drift spin–orbit field. They injected spin polarization optically into a GaAs quantum well and applied an electric field to give a photo-current of these polarized spins. The drift spin–orbit field then drove a precession of the photo-induced spin polarization which could be monitored via the dependence of the polarization of the luminescence on the magnitude of the applied *electric* field. This was effectively a Hanle effect [67] experiment, but with an applied magnetic field augmented by the drift spin–orbit field.

### *3.4. Spin currents*

One may ask whether there is also a spin current associated with the charge current driven by an applied electric field in the presence of the Rashba splitting. It has been shown [58, 68] that for elastic point scatterers, the answer is no. The result may be seen easily, in the clean limit, for the model of non-interacting electrons that we have used here. Figure 4 contrasts several non-equilibrium situations, with the equilibrium Fermi circles indicated by dotted lines, the non-equilibrium by solid lines. The bold arrows indicate added occupation and the dotted arrows depleted occupation, as compared with the equilibrium situation. We compare the spin-split cases 4(a) and (b) with the cases 4(c) and (d) for material with no spin splitting. In 4(a) and (c) we have displaced Fermi discs, e.g., the result of application of an in-plane electric field, with no repopulation from one disc to the other. Figure 4(a) illustrates the example discussed already, with charge current and spin polarization. The displacement of the discs

has enhanced the spin-down population of disc 1 and depleted that of disc 2. The presence of the spin splitting prevents full cancellation, since the densities of the states of the two bands, equation (22), are in the ratio $k_1/k_2 = (1+\eta)/(1-\eta)$. If we ask for the non-equilibrium spin current in disc 1 we find that there is a positive spin-down current associated with the excess of down spins with positive velocity. On the other hand there is also a *deficit* of *up* spins with *negative* velocity. The net result of the three italicized words is a negative contribution to the spin-down current, cancelling the more obvious positive contribution from the down spins. For 4(c) we have charge current but neither spin polarization nor spin current: in the absence of correlation of spin and wavevector of the eigenstates, the charge and spin degrees of freedom are uncoupled.

In cases figures 4(b) and (d) we have displaced carriers from one Fermi disc to the other but left them undisplaced in $k$. The effect of the departure from equilibrium now is to give a spin current (but no spin polarization) for the spin-split bands in figure 4(b), and spin polarization (but no spin current) for the unsplit bands of figure 4(d). We mention briefly, in section 5.4, experimental results [69] using interference of a pair of optical beams in which spin current is generated in the absence of charge current.

A simple calculation shows that there are counter-intuitive contributions to a spin current from each disc *in equilibrium* which sum to a total spin-current density of $3n\eta v_F/4 = 3n\alpha/4\hbar$ cm$^{-1}$ s$^{-1}$. Of course, as with equilibrium diamagnetic currents, it is not possible to do anything useful with these equilibrium spin currents. For a Rashba symmetry their presence should be manifested, however, as torques on the host lattice at the boundaries of the 2DEG, the torques being parallel to the boundary and in the plane of the interface. At these boundaries there is reflection of the carriers with a concomitant spin flip: angular momentum must be provided by the lattice which then feels a reaction torque. One can make a rough estimate of the deformation, resulting from this torque, for a cantilever of thickness 0.1 $\mu$m and length 1 mm containing a spin-split 2DEG. With current technology the predicted displacement of the end of the beam of 1 Å could be easily measured by modulating the spin splitting with a gate, but the effect would presumably be completely masked by much larger electrostatic and piezoelectric induced deflections.

## 4. Detection of current induced spin polarization

### *4.1. Ferromagnetic spin probes*

Having noted that a spin polarization can be induced by an electric field, it is natural to ask whether that spin polarization can be detected by some electrical probe. In 1976 Aronov [70] suggested that excess spins could be injected into a paramagnetic metal by passing an electric current into the metal from a ferromagnetic conductor. This idea prompted Silsbee [71], in 1980, to propose the use of a ferromagnetic probe to detect the non-equilibrium spin polarization of a conductor. The validity of the proposal was verified in experiments of Johnson [72] and later by van Son *et al* [73] using a pair of ferromagnetic electrodes: one to serve as an injector of non-equilibrium spin density, the other to detect it. Johnson [59], in 1998, suggested the use of a ferromagnetic probe to detect the spin polarization produced by a charge current in a 2DEG with spin splitting in the conduction band. The ideas were confirmed in a series of papers with Hammar *et al* [74–78]. A phenomenological theory of the experiment was presented by Silsbee [64, 65].

*4.1.1. Spin detection.* Figure 5 illustrates the basic idea of spin detection in a paramagnetic 2DEG without spin splitting, using an idealized ferromagnetic probe containing only a single

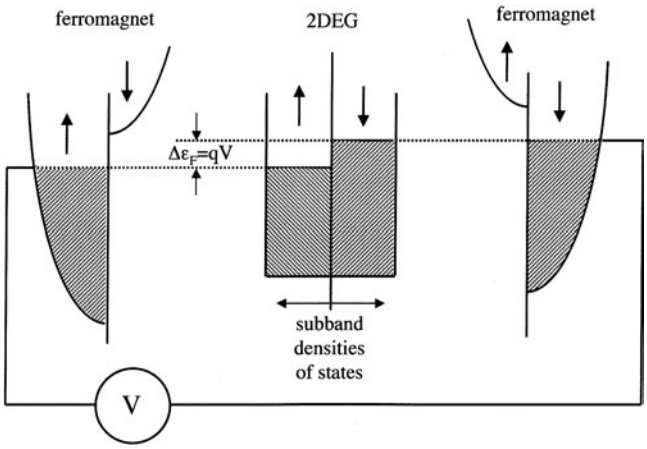


**Figure 5.** Schematic of the detection of spin polarization of a paramagnetic material using ferromagnetic potential probes.

spin subband, a 'half-metal ferromagnet'. It is a picture that is also appropriate for spin-split systems in the dirty limit, thinking in terms of spin-up and -down subbands with rapid momentum scattering within each and only slow DP relaxation between the two. At the centre is the density-of-states plot for the two spin subbands of the 2DEG in zero magnetic field. We suppose a non-equilibrium spin polarization $P$ is maintained by some injection technique in the 2DEG as evidenced by the difference $\Delta\epsilon_{\mathrm{F}}$ in the pseudo-Fermi levels of the two spin subbands with $\Delta\epsilon_{\mathrm{F}} = 2P\epsilon_{\mathrm{F}}$.

If no current is allowed to flow in the external circuit, and if there is no spin relaxation at the interface, there will be charge flow of spin-down carriers between the spin-down ferromagnet on the right and the spin-down subband of the paramagnet until the Fermi levels match, as illustrated. Similarly the ferromagnet on the left equilibrates with the spin-up pseudo-Fermi level of the paramagnet. The voltmeter, drawing no current, measures the difference between the Fermi levels of the two ferromagnetic probes,

$$V = \frac{\Delta\epsilon_{\mathrm{F}}}{q} = 2\frac{\epsilon_{\mathrm{F}}}{q}P. \tag{23}$$

For a typical ferromagnet with a Fermi level cutting both spin subbands the voltage will be reduced, since the Fermi level will now equilibrate to a weighted average of the two pseudo-Fermi levels of the paramagnet. The weighting factors depend on the details of the boundary conditions at the interface and the densities of states and conductivities of the two subbands of the ferromagnet [79]. For high impedance junctions the weighting depends on the relative junction conductances for the two spin orientations.

For low impedance junctions, the subband conductivities and spin relaxation time in the ferromagnet, along with the semiconductor conductivity and spin relaxation time, are the issues. Even though there is no net charge current for a potentiometric probe there can be compensating spin currents across the interface which disturb the magnetization within the paramagnet. Closely related to the effect of these partial currents on the detector efficiency is the problem of injection efficiency from a low resistivity ferromagnet through a low impedance junction into a semiconductor or 2DEG [80–82]. For the moment we consider only the case in which the junction impedance is sufficiently large that these partial currents do *not* disturb the spin distributions in either ferromagnet or paramagnet.

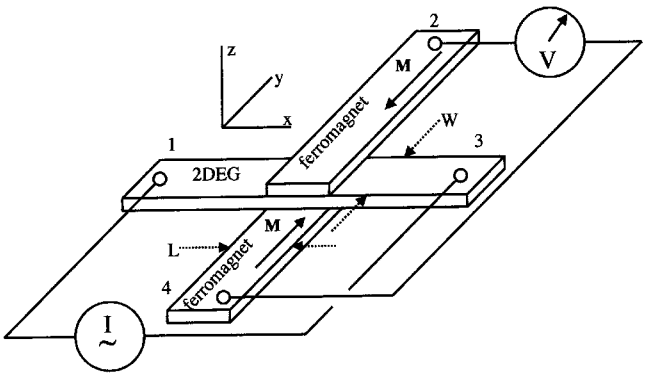


**Figure 6.** Conceptual experiment for the electrical detection of electric-field induced spin polarization.

Adopting this assumption we introduce a parameter $m$ reflecting the degree of spin asymmetry of the ferromagnet–paramagnet junction: in the simplest of models it might represent the magnetization of the ferromagnet normalized to the maximum possible if all spins were parallel. Equation (23) is then replaced by

$$V = \frac{2m\epsilon_{\mathrm{F}}}{q} P. \tag{24}$$

For the slow scattering, or clean, limit there is no longer a well defined pseudo-Fermi level for each spin orientation. Referring to figure 3(a) we see that we can relate the spin polarization and charge current to the shifts of the discs or, more precisely, to the first moments of the distributions in each of the discs. It is shown in [64] that the Fermi level of the ferromagnetic probe, in the limit of high junction impedance, is a measure of difference of these first moments, hence of the spin polarization.

*4.1.2. The experiment.* Figure 6 defines a conceptual experiment, convenient for illustration, in which a current is driven through a 2DEG in the $x$-direction to produce a spin polarization in the negative $y$-direction via the mechanism of section 3. A pair of oppositely magnetized ferromagnetic films then probe the non-equilibrium spin distribution of the 2DEG giving a signal voltage through the mechanism described above. Equations (21$b$) and (24) are combined to give an estimate of the voltage $V$ induced in the ferromagnetic probe by the spin polarization associated with the current density $j = I/W$, where $I$ is the drive current and $W$ the width of the 2DEG:

$$V = 2m\eta R_\lambda I = m\frac{\alpha k_{\mathrm{F}}}{\epsilon_{\mathrm{F}}} R_\lambda I, \tag{25}$$

with

$$R_\lambda = \frac{2\pi\hbar}{q^2}\frac{1}{Wk_{\mathrm{F}}} = \frac{\lambda}{W\sigma}. \tag{26}$$

The resistivity mean free path is $\lambda = v_{\mathrm{F}}\tau$ and we have used the form $\sigma = q^2\lambda k_{\mathrm{F}}/2\pi\hbar$ for the electrical conductivity of the 2DEG. As long as the junction impedance is sufficiently high this result is valid independent of the length $L$ of the junction, i.e. the width of the ferromagnetic film in figure 5 [64].

The resistance $R_\lambda$ characterizing the linear response in this system is expressed, in the first form in equation (26), as $\pi/2$ times the inverse of the parallel quantum conductance of the

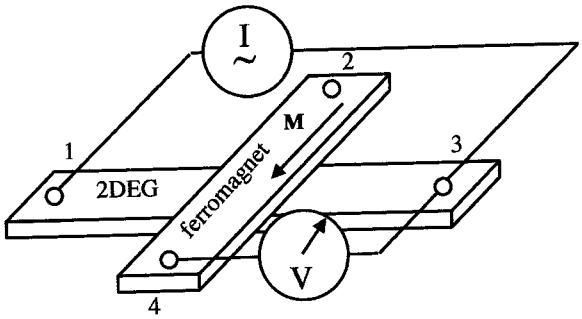


**Figure 7.** Sample configuration for the 'potentiometric' experiment of Hammar *et al*. The 'diode' experiment uses the same geometry, but with the current driven from terminal 1 to terminal 2.

$2Wk_F/\pi$ transverse modes of the 2DEG channel of width $W$, and in the second form, as the resistance of a length of the channel equal to the mean free path $\lambda = v_F\tau$. The 'signal resistance' $V/I$ is then predicted to be $2R_\lambda$ reduced by the dimensionless parameters $m$ characterizing the spin asymmetry of the junction and $\eta = \alpha k_F/2\epsilon_F$ characterizing the strength of the spin–orbit splitting.

Experiments of Hammar, Johnson *et al* [75–78] in the geometry of figure 7 have used a 15 nm wide InAs 2DEG confined by AlGaAs barriers. The experiments used only a single permalloy film as a probe rather than the conceptually simpler configuration of figure 6. The voltage between terminals 4 and 3, including contributions from both the spin-dependent electrochemical potentials and the regular ohmic resistance drops in the region of the junction, was measured for the magnetization of the film in each of the positive and negative $y$-directions. Taking the difference of these two measured voltages eliminates the contributions from the ohmic resistance drops, which are independent of magnetization direction. This gives a result equivalent to the single measurement in the conceptual experiment of figure 6 with the pair of ferromagnetic probes. The lower curve and left-hand scale of figure 8 [77] show the measured ratio of voltage to drive current as a function of an applied field in the $y$-direction. The signal depends only weakly upon field until the magnetization reversals at about $\pm 30$ Oe. The step height of about 0.4 $\Omega$ reflects the change in ferromagnetic Fermi level as its magnetization is changed from parallel to antiparallel to the electric-field induced spin polarization.

Was the observed magnitude of signal appropriate? Unfortunately neither the strength of the Rashba splitting nor the efficiency $m$ of the spin detection were independently measured. Although $m$ may depend upon chemical complexities of the interface [83] or crystal orientation, the value of $m = 0.4$, based on ferromagnet-superconductor tunnelling experiments [84], is commonly used for permalloy in absence of more specific information. Using this value for the permalloy film and equation (25) gave a Rashba constant $\alpha = 2 \times 10^{-9}$ eV cm$^{-1}$. The agreement with the values of $\alpha$, for InAs wells, collected in table 1 certainly implies consistency of the experiment with theory within the uncertainties of the system parameters.

As noted earlier, for low junction impedance the partial currents, corresponding to up-spin and down-spin flow between the 2DEG and the ferromagnet, perturb the spin-polarization distribution within the 2DEG, decreasing the observed signal. Does this observation cast doubt on the experimental results? In the clean limit, the numerical simulations of [64, 65] show the critical parameters to be the ratio $G$ of the junction conductance to the conductance $R_\lambda^{-1}$ characterizing the 2DEG and the ratio of junction length to mean free path. If the normalized conductance $G$ is smaller than unity, equation (25) is valid for a wide range of junction lengths $L$. For low impedance junctions, large $G$, the signal becomes exponentially small in $G$ at a rate which increases with increasing ratio of junction length $L$ to the mean free path $\lambda$.

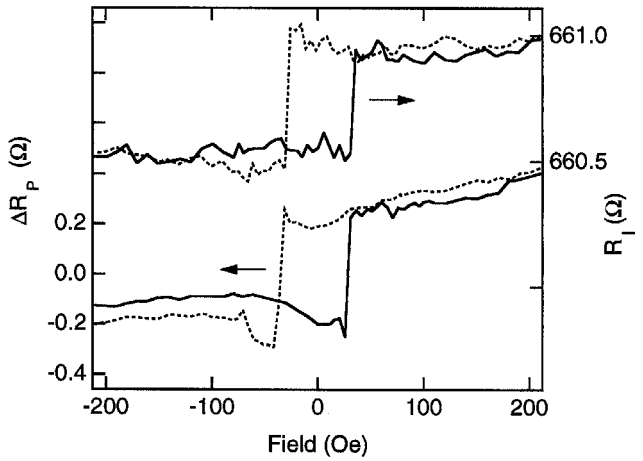


**Figure 8.** Data of Hammar *et al*. Lower curve, left-hand scale: the measured resistance $V_{43}/I_{13}$, with background subtracted, *versus* applied magnetic field for the 'potentiometric geometry'. Upper curve and right-hand scale: the measured resistance $V_{43}/I_{12}$ *versus* applied magnetic field for the 'diode geometry'.

These predictions are consistent with the Hammar–Johnson experiments with samples with different junction impedances as discussed in [77]. The junction conductances in all of their samples are in or near the high impedance limit.

### *4.2. Other detection options*

Circular polarization of photo-luminescence has been suggested by Ivchenko and Pikus [53] as an alternative method of detecting electric-field induced spin polarization. Carriers *without* spin polarization are excited optically with unpolarized light and driven with an applied electric field. Associated with the current, then, should be an electric-field induced spin polarization of magnitude given by equation (21*a*). The proposal of [53] is to detect the spin polarization through analysis of the circular polarization of the recombination luminescence.

Aronov and Lyanda-Geller [54] proposed detecting the induced spin polarization through nuclear magnetic resonance (NMR) excitation by an alternating electric field. The alternating electric field would excite an oscillatory spin polarization, via the spin–orbit mechanism, which would couple in turn to the nuclei, via hyperfine interaction, and serve as a driving mechanism for the nuclear resonance. Edelstein [56] suggested an alternative NMR scheme for the Rashba case in which a constant electric field, perpendicular to the applied magnetic field of the NMR experiment, induces a shift of the NMR resonance via the electric-field induced spin polarization combined with the electron-nuclear hyperfine interaction.

Chaplik *et al* [57] have also evaluated the feasibility of direct detection of the flux generated by the aligned spins using SQUID magnetometry. It does not sound easy.

Apparently none of these schemes, optical, NMR, or direct flux measurement, have actually been used to detect the electric-field induced spin polarization unless perhaps the NMR enhancement seen in the experiments of Clark and Feher [85] was the result of some such mechanism.

## 5. From spin polarization to charge current

Having explored the possibility of using a charge current to drive a spin polarization, it is only natural to ask about the converse situation: will the presence of a spin polarization result in a charge current? The following argument suggests the answer is yes.

We may prepare a spin polarized state of a 2DEG-Rashba system easily by application of a magnetic field, say, in the negative $y$-direction. Figure 3(b) shows the equilibrium configuration of the Fermi discs after inclusion of the Zeeman energy

$$E_{\mathrm{Z}}(\boldsymbol{k}) = \mp\frac{g\beta H}{2}\frac{k_x}{k}, \tag{27}$$

with the upper sign for disc 1 and the lower for disc 2. The term $k_x/k$ arises from the projection of the applied field onto the quantization direction of the spins in state $\boldsymbol{k}$. Spin polarization results from the transfer of spin-up electrons from one side of each of the Fermi discs to spin-down states on the other. The resulting displacement of the Fermi discs,

$$\delta k = \frac{g\beta H}{2}\frac{k_{\mathrm{F}}}{2\epsilon_{\mathrm{F}}}, \tag{28}$$

gives the conventional Pauli paramagnetism. The figure also *suggests* that in equilibrium there is charge current in disc $i$ given by

$$j_i = \frac{qk_i v_{\mathrm{F}}}{4\pi}\delta k. \tag{29}$$

However, adding the contribution to the group velocities from the $k$ dependence of the Zeeman energy,

$$v_{\mathrm{Z}x}(\boldsymbol{k}) = \frac{1}{\hbar}\frac{\partial E_{\mathrm{Z}}(\boldsymbol{k})}{\partial k_x} = \mp\frac{g\beta H}{2\hbar}\frac{k_y^2}{k^3}, \tag{30}$$

avoids this embarrassment by cancelling the contributions from equation (29). Of course, we can expect a charge current only as a consequence of *non*-equilibrium spin polarization.

Suppose now the magnetic field is quickly removed: for times short compared with the resistivity scattering time $\tau_\rho$, the distribution is still described by figure 3(b). However there now *is* a charge current simply related to the displacements of the discs and which corresponds to the sum over the occupied states of carrier charge $q$ times the 'Zeeman velocity' given by equation (30), or equivalently by equation (29). In contrast with figure 3(a) we have here the two Fermi discs shifted in *opposite* directions by an equal magnitude $\delta k = g\beta H k_{\mathrm{F}}/4\epsilon_{\mathrm{F}}$. We may now compute the magnitudes of the non-equilibrium current and spin for each of the discs. Adding the partial spin densities and the partial currents and combining we obtain the results which are the converse of equation (21*b*)

$$P = \frac{\delta k}{k_{\mathrm{F}}} \tag{31}$$

$$j = \frac{\delta k}{k_{\mathrm{F}}} nq v_{\mathrm{F}}\eta = nq v_{\mathrm{F}}\eta P = nq\frac{\alpha}{\hbar}P. \tag{32}$$

For the individual discs we have the charge–current density to spin-polarization ratio equal to $nq v_{\mathrm{F}}$. When combining the contributions from the two discs the imbalance of the cancellation is characterized by the parameter $\eta$ which appears on one or the other side of the ratio as seen in equations (21*b*) and (31). This reflects the relative shifts of the discs seen in figures 3(a) and (b). (The factor of two in the first form of equation (21*b*), specific to the particular scattering model, is irrelevant to this rough comparison of the two results.)

In the discussion of the charge–current induced spin polarization, the experimental challenge is to find a satisfactory method to detect the spin polarization. For the converse problem, the measurement of the induced current is straightforward and the experimental issue becomes finding a more practical means of producing the non-equilibrium spin polarization than the conceptual scheme proposed above.

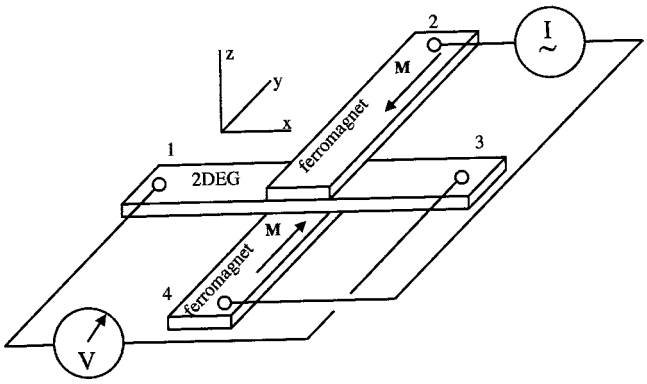


**Figure 9.** Conceptual experiment for the electrical detection of current driven by electrical injection of spin polarization.

### *5.1. Electrically injected spin polarization*

In principle, a quite simple experiment to demonstrate the polarization induced current is the converse of the Hammar–Johnson potentiometric experiments [77] as illustrated conceptually by figure 9. A current is driven from a ferromagnetic electrode 2 magnetized antiparallel to $\hat{\boldsymbol{y}}$ through the centre portion of a bar of 2DEG into a ferromagnetic electrode 4 magnetized parallel to $\hat{\boldsymbol{y}}$. We suppose a spin–orbit splitting of the Rashba symmetry. This configuration will result in the injection of a non-equilibrium spin polarization in the negative $y$-direction into the 2DEG as suggested by Aronov [70] and as demonstrated in a metallic system by Johnson and Silsbee [72, 79]. The correlation of spin with wavevector implied by the Rashba form of spin–orbit splitting implies that this injected polarization will be associated with a charge current in the $x$-direction. We then predict a current in a zero impedance ammeter connecting terminals 1 with 3. Alternatively we might measure the voltage induced with an infinite impedance voltmeter. Imposition of zero current boundary conditions at the ends of the 2DEG results in the build up of space charge within the 2DEG, inducing a current which cancels the injected charge current, the integral of the space charge field over the length of the 2DEG giving the measured voltage.

Again we assume the impedance of the junctions between the 2DEG and the injecting electrodes to be large enough to be in the high impedance limit defined in [64]. Further the width of the injecting electrode $L$ is taken as large compared with the spin-diffusion length $\lambda_S$ in the 2DEG. We investigate the response to a charge flow of $\delta n_{\rm inj}$ carriers per unit area from electrode 2 to 3 in a time short compared with all characteristic times in the 2DEG. The effect will be to inject a spin density parallel to the $y$-direction of magnitude $2m\delta n_{\rm inj}(1/2)$ per unit area; the factor of two due to the spin injection from *both* electrodes: current out through a spin-up ferromagnet injects the same sign of spin density as current in through a spin-down ferromagnet. $m$ is again a measure of the spin asymmetry of the ferromagnet–2DEG junction. Immediately after injection the corresponding increment in polarization will be

$$\delta P_y = 2m\delta n_{\rm inj}/n. \tag{33}$$

The probability that an injected carrier with spin down goes into a given $\boldsymbol{k}$-state in the 2DEG is proportional to the square of the spin projection onto the spin states associated with $\boldsymbol{k}$. Hence spin-down carriers are more likely to go into states of positive $k_x$ in disc 1 and states of negative

$k_x$ in disc 2. This argument leads to the expression for the injected current increment,

$$\delta j_{xi} = m\delta n_{\rm inj} q \frac{k_i}{2\pi k_{\rm F}} \int_0^{2\pi} {\rm d}\theta\, v_{\rm F} \cos\theta (1 \pm \cos\theta) \tag{34}$$

$$= \pm m\delta n_{\rm inj} q v_{\rm F} \frac{(1 \pm \eta)}{2}, \tag{35}$$

with the factor $(1 \pm \cos\theta)$ in the integral around the Fermi circle coming from the square of the spin projections. This is an injection of a current increment, *not* of charge. The full charge $q\delta n_{\rm inj}$ flows from one ferromagnet to the other, but this charge is injected into or drawn from different portions of the Fermi discs to leave a net current in the 2DEG. This net increment in current density in the 2DEG is

$$\delta j_x = \delta j_{x1} + \delta j_{x2} = m\eta\delta n_{\rm inj} q v_{\rm F} = \frac{nq v_{\rm F} \eta \delta P_y}{2}. \tag{36}$$

To follow the subsequent evolution of the system we look separately at the two limits of the DP relaxation.

*5.1.1. Clean limit.* After injection, the spin polarization and current begin to decay. The first process, in the time interval $\omega_{\rm SO}^{-1} \ll t \ll \tau$, is the precession of the spins in their individual spin–orbit fields at the rate $\omega_{\rm SO}$: only the component of spin parallel to the quantization axes illustrated in figure 2 is preserved. This precession reduces the polarization by a factor of two in a time of order $\omega_{\rm SO}^{-1}$, but leaves the current increment intact. At longer times the spin and current increments decay simultaneously with the time constant $\tau$. Under continuous injection of current $I = \delta j_{\rm inj}$ into the junction area $WL$ we deduce a steady-state accumulation of polarization and current density

$$P_y = \frac{mI}{nqWL}\tau \qquad \text{and} \qquad j_{x\,\rm inj} = \frac{m\eta I \tau v_{\rm F}}{WL}. \tag{37}$$

The ratio $\delta j_x / \delta P_y$ is as given by equation (32).

In the experiment suggested by figure 9 this current is cancelled by a reverse current driven by a space charge field $\mathcal{E}_{\rm sc} = j_{x\,\rm inj}/\sigma$ associated with a potential barrier of height $V = \mathcal{E}_{\rm sc} L = \eta m R_\lambda I$, which will be the magnitude of the open circuit voltage between terminals 1 and 3. This result differs by a factor of two from that obtained using the scattering model of [64]. Inclusion of the more realistic scattering gives a faster scattering rate for the smaller disc, hence less current contribution from this disc and a larger total steady state current to restore this factor of two,

$$V = \mathcal{E}_{\rm sc} L = 2\eta m R_\lambda I. \tag{38}$$

*5.1.2. Dirty limit.* If we follow the fate of the injected spin and current introduced in section 5.1 we find a different picture in the dirty limit. Now the spin is remembered on the timescale of $\tau_{\rm S}$ while the current decays in a time $\tau_\rho$. The resulting accumulated spin polarization and current with steady injection would become

$$P_y = \frac{2mI}{nqWL}\tau_{\rm S} \qquad \text{and} \qquad j_{x\,\rm inj} = \frac{m\eta I \tau_\rho v_{\rm F}}{WL} = \frac{\eta n q v_{\rm F}}{2} \frac{\tau_\rho}{\tau_{\rm S}} P_y. \tag{39}$$

The corresponding open circuit voltage is

$$V = \mathcal{E}_{\rm sc} L = \frac{j_{x\,\rm inj}}{\sigma} L = \eta m R_\lambda I, \tag{40}$$

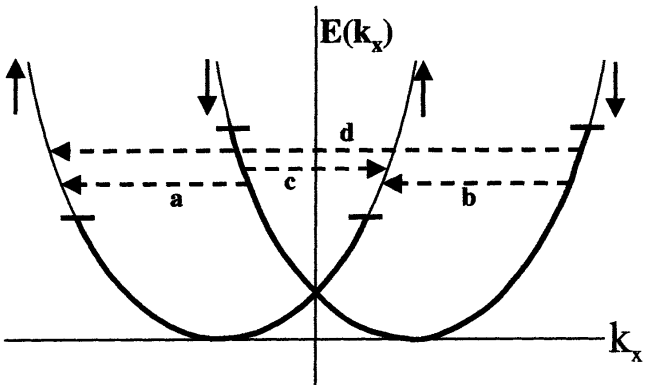


**Figure 10.** Spin-flip scattering as a source of spin induced charge current. Dashed arrows indicate various allowed spin relaxation processes.

within a factor of two the same as equation (38). Although the current to spin ratio is reduced by $\tau_\rho/\tau_S$, the higher resistivity of the 2DEG, proportional to $\tau_\rho$, gives a voltage signal independent of $\tau_\rho$.

Now, however, there is a second contribution to the current, this one associated with the spin-flip scattering processes and first suggested in conjunction with photo-excitation of spin polarization by Ivchenko *et al* [86, 87] in 1989. Consider the transient response to a brief injection of spin and current: after a time of several $\tau_\rho$ the injected current has decayed but not the spin. The picture is then as illustrated by figure 10 with a spin-up and a spin-down subband filled to different pseudo-Fermi levels but carrying no charge current. Note that in this picture, appropriate to the dirty limit, the spins are quantized according to their direction during the injection process and, after several $\tau_\rho$, are *no longer* correlated with their wavevector.

Next consider the four spin relaxation events indicated in figure 10 by the arrows [103]. Events 1 and 2 transfer carriers between states of the same velocity and hence do not alter the charge current. Events 3 and 4, however, change the direction of the carrier velocity. Though the two tend to cancel, they involve different changes $\Delta k$ in wavevector and, as long as the scattering probability depends on $\Delta k$ the cancellation will be incomplete. On average, each event will contribute to the current a term of order $\eta q v_F/L$ for a time $\tau_\rho$.

The spin-relaxation scattering events occur at a rate $nP/\tau_S$ and in steady state, with generation balanced by resistivity scattering, give a relaxation driven current of magnitude

$$j_{\text{kinetic}} = \eta n q v_F \frac{\tau_\rho}{\tau_S} \xi P, \tag{41}$$

where $\xi$ is a parameter of order unity determined by the $\Delta k$-dependence of the spin-flip scattering. The subscript 'kinetic' is the term coined by Ivchenko *et al* [87] to distinguish this source of current from that associated with the preferential photo-excitation of carriers with a net velocity, their 'relaxational' mechanism. Equation (41) differs from the ratio $j_{\text{inj}}/P$ given by equation (39) only by the factor $2\xi$: the two contributions to the steady state are comparable in magnitude.

In principle they may be distinguished from the transient response. If the injecting current could be turned off in a time short compared with $\tau_\rho$ the subsequent charge current decay would show two components. The injection, or relaxational, contribution would decay with a time $\tau_\rho$, that from the kinetic contribution with time $\tau_S$. We will see an alternative way to distinguish the two in section 5.3.

*5.1.3. Experimental result.* Hammar *et al* [74–78] have also performed measurements, using a single ferromagnetic film, equivalent to that defined by figure 9 with the pair of films. In their 'diode geometry' a current is driven from the 2DEG into the ferromagnet, via arms 1 and 2 in figure 7 and the voltage is measured between arms 3 and 4. Again the 'signal voltage' is the difference between these two voltages resulting from a reversal of sign of the magnetization of the ferromagnet. The experiment defined by figure 9 with two ferromagnets may be represented as a linear superposition of two of the diode-geometry experiments with reversed magnetizations and currents. Simple manipulations show that the $\Delta V$ of the diode experiment is the measured voltage of the conceptual converse experiment, the electrical detection of injected spin polarization.

The upper plot in figure 8 shows the resistance signal $V_{43}/I_{12}$ as a function of applied magnetic field for the 'diode' geometry. The step in signal with magnetization reversal is the same as for the potentiometric case. It is perhaps surprising to see the same result for the two, apparently quite different, experiments. This equality is, however, predicted as seen by equations (38) and (25). Comparison of figures 6 and 9 shows that the two conceptual experiments differ only in the exchange of current and voltage leads. The Onsager reciprocity relations [88, 89] assure that these two results are identical. The numerical calculations [64, 65] are fully consistent with Onsager requirement, independent of junction length and impedance.

To apply the Onsager relations to the actual experiments it is necessary to assume the resistance of the ferromagnetic film in the junction region to be small compared to the junction resistance: this condition was well satisfied for the sample used for figure 8 [77, 65]. It is essential to recognize that the experiment in the diode geometry is a three terminal measurement and that the signal measured between arms 3 and 4 is *not* a measure of the junction impedance that would be measured between arms 1 and 2, a two terminal measurement. Although we have assumed constant electrochemical potentials in the low resistivity ferromagnetic film in the junction region, we *must* consider variations in the potentials in the 2DEG. The observed signal results from magnetization dependent buildup of space charge and associated potential variations within the 2DEG in the region of the junction, *not* from a magnetization dependence of the two terminal junction resistance. As pointed out by van Wees [90] and others [91, 58, 92], Onsager assures us that the two terminal resistance cannot change with reversal of the sign of the magnetization.

The first experiment of Hammar *et al* [74], which used exclusively the diode geometry, was called into question by van Wees [90] on the basis of the apparent violation of the Onsager symmetry. The criticism was appropriate for the language used to interpret the experiment, which made frequent reference to measurement of the interfacial resistance. As noted in the preceding paragraph, the configuration used in [74] is *not*, as stated in [74], 'a standard four-probe configuration for measuring interface resistance' between the ferromagnet and the 2DEG. The criticism of van Wees is thus appropriate to the original interpretation of the experiments, but does *not* call into question the validity of the experimental results as a measurement of the electrical detection of electrically injected spin polarization.

Monzon *et al* [93] have criticized the experiment primarily on experimental grounds. They expressed suspicion of the results based on the lack of success of experiments by many authors to demonstrate spin injection into semiconductors from metallic probes. As noted earlier, inefficient injection (and detection) is an expected consequence of the combination of the large disparity in conductances of the two materials *and* a low junction impedance. Estimates show that the junction impedance in the challenged experiment was sufficiently high to obviate this problem. The criticism also suggested that the observed signals were a consequence of Hall effect voltages resulting from micro-fringing fields near the edges of the ferromagnetic film. Additional experiments of Hammar *et al* [94] give convincing evidence against that interpretation.

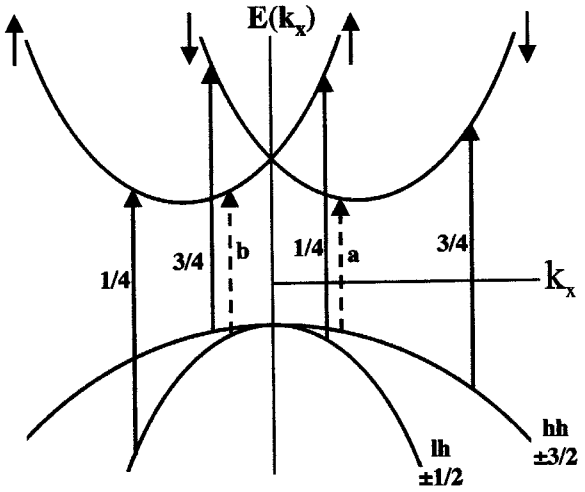


**Figure 11.** Schematic of mechanism of circular photo-galvanic effect for an intrinsic semiconductor. Dashed arrows—threshold transitions; solid arrows—allowed transitions for photon energies above threshold.

### *5.2. Circular photo-galvanic effect (CPGE)*

The injection of spin polarization by circularly polarized light [60, 95] offers an alternative to electrical spin injection in exploring the connection between charge current and spin polarization. In 1978 Ivchenko and Pikus [53] and Belinicher [96] suggested independently that this photo-injection of spin polarization would be accompanied by a charge current. The predictions were quickly confirmed by Asnin *et al* [97, 98] in tellurium with more detailed results reported in 1984 by Averkiev *et al* [99]. There is a host of mechanisms by which irradiation by circularly polarized light can induce a charge current. This phenomenon is generally referred to as the circular photo-galvanic effect (CPGE) and theoretical treatments [5, 87] have typically focused on systems in the dirty limit, $\tau_S \gg \tau_\rho$. Belinicher and Sturman [100] have extensively reviewed the symmetry requirements and mechanisms for the more general photo-galvanic effect (PGE) summarizing the results as of 1980, and two more recent reviews by Ivchenko [101] in 2002 and by Ganichev and Prettl [2] in 2003 have focused on the CPGE in quantum well structures. In view of these extensive reviews we will give here only some hints of the issues involved.

Figures 11 and 12 illustrate two highly simplified examples in which we ignore the confinement induced splitting of the light–heavy hole degeneracy at $\boldsymbol{k} = 0$ and assume a spin splitting linear in $k$ only in the conduction band. In figure 11 we consider an intrinsic sample with no carriers in either band, optical excitation at an energy only slightly larger than the band gap, and a spin splitting of the Rashba symmetry. We simplify, as well, by sketching the ideas in only one dimension in $k$-space.

Near $k = 0$ the states in the heavy and light hole bands behave like an atomic quartet state. The arrows indicate allowed transitions for one circular polarization of light with light propagating parallel to the $y$-direction, the direction chosen for angular momentum quantization. The dashed arrows represent the threshold for interband absorption which occurs at values displaced from $k = 0$ as a consequence of the linear splitting in the conduction band. Because of the curvature of the valence bands, the electron wavevector at threshold is not at the conduction band minimum and the electrons and holes are created in states with equal but

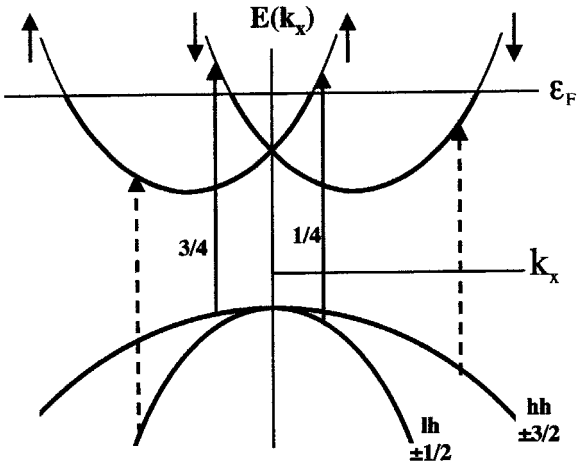


**Figure 12.** Schematic of the mechanism of the circular photo-galvanic effect for a degenerate 2DEG. Dashed arrows—energy allowed but Pauli excluded transitions; solid arrows—energy and Pauli allowed transitions.

opposite finite velocities of magnitude, $v = (\alpha/\hbar)[m_e/(m_e + m_h)]$. Here $m_h$ is the heavy or light hole mass for the transitions marked a and b respectively. The solid arrows correspond to transitions at energies slightly above threshold, with the numbers giving the relative intensities of the four transitions. The stronger transitions from the heavy hole states lead to the excitation of a net spin-down of 1/4 for each photo-excitation. If the carrier lifetime against recombination $\tau_L$ is long compared with the spin relaxation time $\tau_S$ in the steady state we will have

$$P_y = \frac{1}{2n}\frac{dn}{dt}\tau_S = \frac{\tau_S}{2\tau_L}, \tag{42}$$

where $dn/dt$ is the rate of photon absorption, and $n$ the steady state electron concentration.

Although the two transitions from the heavy-hole band, of weight 3/4, give electrons travelling in opposite directions, their average velocity is the same as the velocity of the electron created at threshold $v_a$: in net there will be a negative velocity of the electrons excited from the heavy-hole band. Similarly, excitations from the light-hole band give, on average, electrons with positive velocity. The relative magnitudes of the cancelling terms depend upon the effective masses in the three bands and, in the more realistic case, the relative magnitudes of the Rashba spin splittings in the valence and conduction bands. Also, this one-dimensional picture hides important density of states factors which complicate the situation further. We may write the resulting charge current as

$$j_x = \xi' q \frac{dn}{dt}\tau_\rho \frac{\alpha}{\hbar} = nq\frac{\alpha}{\hbar}\frac{\tau_\rho}{\tau_S}\xi' P_y = \eta n q v_F \frac{\tau_\rho}{\tau_S}\xi' P_y, \tag{43}$$

where $n$ is the steady state photo-electron concentration and $\xi'$ a numerical constant incorporating the partial cancellations of the various contributions to the charge current. This shows a reduction from equation (31), for which spin and resistivity times were implicitly assumed the same, by the factor $\xi'\tau_\rho/\tau_S$: the drift velocity imparted by the optical excitation is destroyed faster than the spin polarization by the factor $\tau_S/\tau_\rho$. A full treatment, for example Golub [102], shows the complexity of the physics and of the spectral response for a more realistic model.

Figure 12 illustrates a similar situation, but now for a degenerate n-type sample, with photon excitation at an energy just above the threshold of $(E_G + \epsilon_F)$. We take the resistivity

scattering rate to be sufficiently low that the spin splitting energy is well resolved, the clean limit of section 3.1. The four arrows indicate energetically allowed transitions of which the dashed arrows are forbidden by the exclusion principle: transitions are allowed only to the inner of the two Fermi discs. Again the selection rules favour excitation of spin-down electrons, now unambiguously with negative group velocity. Using a Rashba-symmetry correlation of spin with wavevector gives for the spin polarization and charge current,

$$P_y = \frac{1}{2n}\frac{\mathrm{d}n}{\mathrm{d}t}\tau \qquad \text{and} \qquad j_x = \frac{q}{2}\frac{\mathrm{d}n}{\mathrm{d}t}\tau v_\mathrm{F}. \tag{44}$$

It is remarkable that equation (44) does *not* involve the spin splitting parameter! The result is valid, however, only for photon energies too small to allow the transitions indicated by the dashed lines in figure 12. For higher energies we are in a situation closer to that of figure 11. The range of photon energies, to first order in $\eta$, for which equation (44) is applicable, is

$$\Delta E_\mathrm{photon} = 4\eta\epsilon_\mathrm{F}\frac{m_\mathrm{e}^*}{m_\mathrm{h}^*}, \tag{45}$$

where the difference between heavy- and light-hole effective masses has been ignored. Again, the prediction for a realistic two-dimensional system which properly includes splitting of the light–heavy hole mass degeneracy at $k = 0$ by the confinement, and the spin splittings of the valence band requires a much more complex analysis.

### *5.3. Precession injection*

We noted in the discussion of the currents induced by electrical spin injection, section 5.1, that there are two mechanisms involved: first the injection process creates a carrier distribution in which there is both charge current and spin polarization. The two are clearly correlated but one might be reluctant to say it is the spin polarization which is the source of the charge current. The corresponding process with optical excitation, described in section 5.2 is the 'relaxational' mechanism of Ivchenko *et al* [86, 87]. The second is the generation of current in the scattering events associated with the spin-relaxation processes, the 'kinetic' mechanism of Ivchenko *et al*. Comparison of equation (43) with equation (41), also applicable with optical excitation, shows the ratio of current density to spin polarization to be of similar magnitude for the two contributions to the current. As in section 5.1, in principle the two mechanisms are distinguishable by their transient response: the relaxational mechanism is characterized by the time $\tau_\rho$, the kinetic by the time $\tau_\mathrm{S}$. However, the required timescales make suitable experiments difficult.

Ganichev *et al* [103] have avoided the timescale problem with an ingenious experiment in which a spin polarization is established by a process which does *not* involve current injection. Optical pumping with the light incident along the normal $\hat{z}$ to the 2DEG injects a spin polarization perpendicular to the conducting plane. Since no current is allowed by symmetry in this geometry, one has a spin polarization only. However, if a magnetic field is now applied in the $x$-direction, in the plane of the 2DEG, the polarized spins precess in this field away from the normal and develop an in-plane component in the $y$-direction. The kinetic mechanism of [87] then drives a current density of magnitude, equation (41),

$$j_\mathrm{kinetic} = \eta\xi nq v_\mathrm{S}\frac{\tau_\rho}{\tau_\mathrm{F}}P. \tag{46}$$

Since the spin is injected by precession in the applied magnetic field there is no injection of current: the observed current is generated by the kinetic mechanism alone. Ganichev [2] has coined the term spin galvanic effect (SGE) for this generation of current via the spin relaxation.

The dependence of signal on magnetic field yields in addition, via the Hanle [67] effect, a direct measure of the spin relaxation time.

More recently Ganichev *et al* [104] have been able to demonstrate the distinction between CPGE and SGE in another way which does not involve the application of an external magnetic field. The authors use a sample with comparable magnitudes to the Dresselhaus and Rashba splittings and photo-excite carriers from the first to the second subbands. Either the SGE or the CPGE can be made to dominate the photo-galvanic effect by suitable choice of orientation of the incident optical beam. The spectral response of the system for the two geometries clearly confirms the dominance of the predicted mechanism.

### *5.4. Other issues*

In section 2.3 we noted the possibility of the interference of the Rashba and Dresselhaus terms. Although the energy dispersion relations in a 2DEG, with growth along (100), are isotropic for both, they differ in the relation between wavevector and spin quantization axis as seen in figure 2. In particular if both terms are present the effective fields add constructively in the (11) direction and destructively in the $(\bar{1}1)$ direction. This interference is the source of the anisotropy noted in section 2.2 and can be quite dramatic if the strengths of the two interactions are comparable. Ganichev *et al* [31] used an n-type InAs quantum well with an array of electrodes around the perimeter in order to measure the direction of any SGE induced currents. Spin polarization was injected by the spin-precession mechanism [103] with the orientation of the spin in the well being determined by the orientation of the magnetic field. Measurement of the strength and orientation of the SGE induced currents as a function of orientation of the magnetic field allowed the determination of the ratio of Rashba to Dresselhaus coupling of about 2.1.

Although our principal focus has been upon the association of spin polarization and charge current, we might mention a recent experiment in which a *spin* current is optically generated in absence of charge current. Hübner *et al* [69], following a proposal by Bhat and Sipe [105], have demonstrated the ability to create non-equilibrium states with a variety of choices of spin polarization, charge current and spin current using photo-excitation by a coherently related pair of laser beams at frequencies $\omega$ and $2\omega$. The two photon excitation by the first interferes with the one photon excitation of the second to allow more specific selection of the spin and wavevector of the excited state by suitably choosing the polarization of the two beams and their relative phase. In the experiment the laser beams are focused on a 4 $\mu$m spot on a thin film of ZnSe. The resultant photo-luminescence contains spatially separated components with opposite circular polarizations. Determining the location of the luminescence for each polarization they find the centres of luminescence to be displaced from the spot of excitation by $\pm 10$ nm. Up-spins have been injected with one velocity, down-spins with the opposite, giving a net spin current, and hence relative displacement of up and down spins, but no resultant charge current.

We have only touched on a few of the ideas related to the optical excitation of spin-associated photo-currents: the following list indicates the wealth of issues relevant to this subject.

- The optical injection may involve interband excitation, as in the examples above, intraband or Drude transitions or, in quantum confined systems, inter-subband transitions.
- There will be contributions to the spin induced current from both the electron and hole states created in the optical transition: the relative importance of the two depends on relaxation rates of the different carriers.

- Detailed arguments will depend upon whether the system is extrinsic or intrinsic and, if extrinsic, whether the carrier gas is Fermi or Boltzmann.
- The spectral response can serve as a useful test of theoretical predictions.
- Much of the qualitative physics depends upon the relative magnitudes of the many characteristic times involved: spin, resistivity, and energy relaxation times and recombination times.
- Quantitative predictions depend upon relative strengths of different scattering mechanisms: DP, Yafet, Bir-Pikus, optical and acoustical phonon, and impurity.
- Photo-currents injected by circularly polarized light result from a combination of the pumping process, the spin relaxation process and spin-dependent recombination processes; they will all show similar symmetry properties and often similar magnitudes.
- Prediction of the temperature dependence provides an additional challenge.

The reader is referred to [2, 96, 98, 100–102] and to references cited therein for a more detailed discussion of some of these issues and for review of recent experimental results.

## 6. Conclusion

The spin–orbit splitting of the one-electron eigenstates in solids of suitably low symmetry gives rise to a curious coupling between non-equilibrium spin polarization and charge currents. The effects are most evident and of most interest in 2DEGs formed in semiconductor heterostructures. The mere existence of an electric current in a 2DEG produces a spin polarization, detectable by ferromagnetic voltage probes or, in some instances, by circular polarization of luminescence. Conversely, spin polarization induced by either optical or electrical injection may be detected by measurement of the associated currents or voltages. These effects offer new tools for the characterization of semiconductor structures and materials; and the possibility of the useful exploitation of these effects in spintronic devices provides both opportunities and challenges in device development.

*Note added in proof.* Rashba [106] has given serious consideration to the issue of equilibrium spin currents and Mal'shukov *et al* [107] have proposed a method for electrical induction of AC spin currents.

## References


[1] Rashba E I and Sheka V I 1991 *Landau Level Spectroscopy* (Amsterdam: North-Holland) p 131
[2] Ganichev S D and Prettl W 2003 *J. Phys.: Condens. Matter* **15** R935
[3] Dresselhaus G 1955 *Phys. Rev.* **100** 580
[4] Seiler D G *et al* 1970 *Phys. Rev.* B **1** 764
[5] Pikus G E *et al* 1988 *Fiz. Tekh. Poluprov.* **22** 185
Pikus G E *et al* 1988 *Sov. Phys.—Semicond.* **22** 115 (Engl. Transl.)
[6] Bir G L and Pikus G E 1961 *Fiz. Tverd. Tela* **3** 3050
Bir G L and Pikus G E 1962 *Sov. Phys.—Solid State* **3** 2221 (Engl. Transl.)
[7] Rashba E I 1960 *Fiz. Tverd. Tela* **2** 1224
Rashba E I 1960 *Sov. Phys.—Solid State* **2** 1109 (Engl. Transl.)
[8] Bychkov Yu A and Rashba E I I1984 *Pis. Zh. Eksp. Teor. Fiz.* **39** 66
Bychkov Yu A and Rashba E I 1984 *JETP Lett.* **39** 78 (Engl. Transl.)
[9] Rashba E I 1961 *Proc. Int. Conf. Semiconductor Physics (Prague, 1960)* (Prague: Czechoslovakian Academy of Sciences Publishing House) p 45
[10] Rashba E I and Sheka V I 1959 *Fizika Tverdogo Tela: Collected Papers* 2 (Moscow: Academy of Sciences of the USSR) p 162
[11] Casella R C 1960 *Phys. Rev. Lett.* **5** 371
[12] Zawadzki W and Pfeffer P 2004 *Semicond. Sci. Technol.* **19** R1

[13] D'yakonov M I and Kachorovskii V Yu 1986 *Fiz. Tekh. Poluprov.* **20** 178
D'yakonov M I and Kachorovskii V Yu 1986 *Sov. Phys.—Semicond.* **20** 110 (Engl. Transl.)
[14] Eppenga R and Schuurmans M F H 1988 *Phys. Rev.* B **37** 10923
[15] Rashba E I and Sherman E Ya 1988 *Phys. Lett.* A **129** 175
[16] de Andrada e Silva E A *et al* 1994 *Phys. Rev.* B **50** 8523
[17] Jusserand B *et al* 1995 *Phys. Rev.* B **51** 4707
[18] Knapp W *et al* 1996 *Phys. Rev.* B **53** 3912
[19] Foulon Y and Priester C 1992 *Phys. Rev.* B **45** 6259
[20] Rössler U and Kainz J 2002 *Solid State Commun.* **121** 313
[21] Vervoort L *et al* 1997 *Phys. Rev.* B **56** R12744
[22] Vervoort L *et al* 1999 *Semicond. Sci. Technol.* **14** 227
[23] Bychkov Yu A and Rashba E I 1984 *J. Phys. C: Solid State Phys.* **17** 6039
[24] Cartoixa X *et al* 2001 *Superlattices Microstruct.* **30** 309
[25] Engels G *et al* 1997 *Phys. Rev.* B **55** 1958
[26] Schaepers Th *et al* 1998 *J. Appl. Phys.* **83** 4324
[27] Lamari S 2002 *Physica* E **12** 435
[28] de Andrada e Silva E A *et al* 1997 *Phys. Rev.* B **55** 16293
[29] Pfeffer P and Zawadzki W 1999 *Phys. Rev.* B **59** R5312
[30] de Andrada e Silva E A 1992 *Phys. Rev.* B **46** 1921
[31] Ganichev S D *et al* 2003 *Preprint* cond-mat/0306521
[32] Miller J B *et al* 2003 *Phys. Rev. Lett.* **90** 076807
[33] Luo J *et al* 1988 *Phys. Rev.* B **38** 10142
[34] Das B *et al* 1990 *Phys. Rev.* B **41** 8278
[35] Luo J *et al* 1990 *Phys. Rev.* B **41** 7685
[36] Das B *et al* 1989 *Phys. Rev.* B **39** 1411
[37] Dorozhkin S I and Ol'shanetskii E B 1987 *Pis. Zh. Eksp. Teor. Fiz.* **46** 399
Dorozhkin S I and Ol'shanetskii E B 1987 *JETP Lett.* **46** 502 (Engl. Transl.)
[38] Lu J P *et al* 1999 *Phys. Rev.* B **60** 13776
[39] Dresselhaus P D 1992 *Phys. Rev. Lett.* **68** 106
[40] Koga T *et al* 2002 *Phys. Rev. Lett.* **89** 046801
[41] Gauer C *et al* 1996 *Surf. Sci.* **361/362** 472
[42] Störmer H L *et al* 1983 *Phys. Rev. Lett.* **51** 126
[43] Stein D *et al* 1983 *Phys. Rev. Lett.* **51** 130
[44] Schultz M *et al* 1996 *Semicond. Sci. Technol.* **11** 1168
[45] Nitta J *et al* 1997 *Phys. Rev. Lett.* **78** 1335
[46] Grundler D 2000 *Phys. Rev. Lett.* **84** 6074
[47] Heida J P *et al* 1998 *Phys. Rev.* B **57** 11911
[48] Gardelis S *et al* 2000 *Physica* E **6** 718
[49] Matsuyama T *et al* 2000 *Phys. Rev.* B **61** 15588
[50] Datta S and Das B 1990 *Appl. Phys. Lett.* **56** 665
[51] Gui Y S *et al* 2002 *Physica* E **12** 416
[52] Lu J P *et al* 1998 *Phys. Rev. Lett.* **81** 1282
[53] Ivchenko E L and Pikus G E 1978 *Pis. Zh. Eksp. Teor. Fiz.* **27** 640
Ivchenko E L and Pikus G E 1978 *JETP Lett.* **27** 604 (Engl. Transl.)
[54] Aronov A G and Lyanda-Geller Yu B 1989 *Pis. Zh. Eksp. Teor. Fiz.* **50** 398
Aronov A G and Lyanda-Geller Yu B 1989 *JETP Lett.* **50** 431 (Engl. Transl.)
[55] Aronov A G *et al* 1991 *Zh. Eksp. Teor. Fiz.* **100** 973
Aronov A G *et al* 1991 *Sov. Phys.—JETP* **73** 537 (Engl. Transl.)
[56] Edelstein V M 1990 *Solid State Commun.* **73** 233
[57] Chaplik A V 2002 *Physica* E **13** 744
[58] Inoue J *et al* 2003 *Phys. Rev.* B **67** 033104
[59] Johnson M 1998 *Phys. Rev.* B **58** 9635
[60] D'yakonov M I and Perel V I 1971 *Zh. Eksp. Teor. Fiz.* **60** 1954
D'yakonov M I and Perel V I 1971 *Sov. Phys.—JETP* **33** 1053 (Engl. Transl.)
[61] D'yakonov M I and Perel V I 1971 *Fiz. Tverd. Tela* **13** 3581
D'yakonov M I and Perel V I 1972 *Sov. Phys.—Solid State* **13** 3023 (Engl. Transl.)
[62] Fishman G and Lampel G 1977 *Phys. Rev.* B **16** 820
[63] Averkiev N S *et al* 2002 *J. Phys.: Condens. Matter* **14** R271

[64] Silsbee R H 2001 *Phys. Rev.* B **63** 155305
[65] Silsbee R H 2003 *Phys. Rev.* B **68** 159902
[66] Kalevich V K and Korenov V L 1990 *Pis. Zh. Eksp. Teor. Fiz.* **52** 859
Kalevich V K and Korenov V L 1990 *JETP Lett.* **52** 230 (Engl. Transl.)
[67] Hanle W 1924 *Z. Phys.* **30** 93
[68] Kalevich V K *et al* 1994 *Solid State Commun.* **91** 559
[69] Hübner J *et al* 2003 *Phys. Rev. Lett.* **90** 216601
[70] Aronov A G 1976 *Pis. Zh. Eksp. Teor. Fiz.* **24** 37
Aronov A G 1976 *JETP Lett.* **24** 32 (Engl. Transl.)
[71] Silsbee R H 1980 *Bull. Magn. Reson.* **2** 284
[72] Johnson M and Silsbee R H 1985 *Phys. Rev. Lett.* **55** 1790
[73] van Son P C *et al* 1987 *Phys. Rev. Lett.* **58** 2271
[74] Hammar P R *et al* 1999 *Phys. Rev. Lett.* **83** 203
[75] Hammar P R and Johnson M 2000 *Phys. Rev.* B **61** 7207
[76] Hammar P R *et al* 2000 *J. Appl. Phys.* **87** 4665
[77] Hammar P R and Johnson M 2001 *Appl. Phys. Lett.* **79** 2591
[78] Hammar P R and Johnson M 2002 *Phys. Rev. Lett.* **88** 066806
[79] Johnson M and Silsbee R H 1988 *Phys. Rev.* B **37** 5312
[80] Hershfield S and Zhao H L 1997 *Phys. Rev.* B **56** 3296
[81] Schmidt G *et al* 2000 *Phys. Rev.* B **62** R4790
[82] Rashba E I 2000 *Phys. Rev.* B **62** R16267
[83] de Teresa J M *et al* 2000 *J. Magn. Magn. Mater.* **211** 160
[84] Meservey R *et al* 1976 *Phys. Rev. Lett.* **37** 858
[85] Clark W G and Feher G 1963 *Phys. Rev. Lett.* **10** 134
[86] Ivchenko E L *et al* 1989 *Pis. Zh. Eksp. Teor. Fiz.* **50** 156
Ivchenko E L *et al* 1989 *JETP Lett.* **50** 175 (Engl. Transl.)
[87] Ivchenko *et al* 1990 *Zh. Eksp. Teor. Fiz.* **98** 989
Ivchenko *et al* 1990 *Sov. Phys.—JETP* **71** 550 (Engl. Transl.)
[88] Onsager L 1931 *Phys. Rev.* **38** 2265
[89] Silsbee R H 2003 *Phys. Rev.* B **68** 153312
[90] van Wees B J 2000 *Phys. Rev. Lett.* **84** 5023
[91] Molenkamp L W *et al* 2001 *Phys. Rev.* B **64** 121202
[92] Bruno P and Pareek T P 2001 *Preprint* cond-mat/0105506
[93] Monzon F G *et al* 2000 *Phys. Rev. Lett.* **84** 5022
[94] Hammar P R *et al* 2000 *Phys. Rev. Lett.* **84** 5024
[95] D'yakonov M I and Perel V I 1984 *Optical Orientation* (Amsterdam: North-Holland) p 11
[96] Belinicher V I 1978 *Fiz. Tverd. Tela* **20** 2955
Belinicher V I 1978 *Sov. Phys.—Solid State* **20** 1706 (Engl. Transl.)
[97] Asnin V M *et al* 1978 *Pis. Zh. Eksp. Teor. Fiz.* **28** 80
Asnin V M *et al* 1979 *JETP Lett.* **28** 74 (Engl. Transl.)
[98] Asnin V M *et al* 1979 *Solid State Commun.* **30** 565
[99] Averkiev N S *et al* 1984 *Fiz. Tekh. Poluprov.* **18** 648
Averkiev N S *et al* 1984 *Sov. Phys.—Semicond.* **18** 402 (Engl. Transl.)
[100] Belinicher V I and Sturman B I 1980 *Usp. Fiz. Nauk* **130** 415
Belinicher V I and Sturman B I 1980 *Sov. Phys.—Usp.* **23** 199 (Engl. Transl.)
[101] Ivchenko E I 2002 *Phys—Usp.* **45** 1299
[102] Golub L E 2003 *Phys. Rev.* B **67** 235320
[103] Ganichev S D *et al* 2002 *Nature* **417** 153
[104] Ganichev S D *et al* 2003 *Phys. Rev.* B **68** 081302
[105] Bhat R D R and Sipe J E 2000 *Phys. Rev. Lett.* **85** 5432
[106] Rashba E I 2003 *Phys. Rev.* **68** 241315
[107] Mal'shukov A G *et al* 2003 *Phys. Rev.* **68** 233307